Fracture compliance estimation using borehole tube waves

GEOPHYSICS, VOL. 78, NO. 4 (JULY-AUGUST 2013); P. D249–D260, 15 FIGS.
10.1190/GEO2012-0521.1

Fracture compliance estimation using borehole tube waves

Sudhish Kumar Bakku[1], Michael Fehler[1], and Daniel Burns[1]

ABSTRACT

We tested two models, one for tube-wave generation and the other for tube-wave attenuation at a fracture intersecting a borehole that can be used to estimate fracture compliance, fracture aperture, and lateral extent. In the tube-wave generation model, we consider tube-wave excitation in the borehole when a P-wave is incident on the fracture. The amplitude ratio of the pressure due to the tube wave to that of the incident P-wave is a function of fracture compliance, aperture, and length. Similarly, the attenuation of a tube wave in the borehole as it crosses a fracture intersecting the borehole is also a function of fracture properties. Numerically solving the dispersion relation in the fracture, we study tube-wave generation and the attenuation coefficient as a function of frequency. We observed that measuring amplitude ratios or attenuation near a transition frequency can help constrain the fracture properties. The transition frequency corresponds to the regime in which the viscous skin depth in the fracture is comparable to its aperture. Measurements in the high-frequency limit can place a lower bound on fracture compliance and lateral extent. We evaluated the applicability of the tube-wave generation model to a previously published VSP data set and found that compliance values of the order 10^{-10}–10^{-9} m/Pa are likely in the field. These observations support scaling of fracture compliance with fracture size.

INTRODUCTION

Naturally occurring fracture networks account for significant fluid flow in many petroleum reservoirs, especially in carbonate reservoirs and other less porous formations. Fracture networks also play an important role in the economic recovery of geothermal energy and for CO_2 sequestration. To model flow in fractured reservoirs, we need to know fracture network properties such as the dominant orientation of the fractures, fracture spacing, and fracture fluid transmissivity. Direct measurement of some fracture properties is possible in boreholes. Borehole televiewer and formation microimager (FMI) logs are the most popular tools for characterizing fractures that intersect boreholes. These logs provide the orientation and spacing of those fractures intersecting the borehole. However, from these data, it is hard to differentiate between fractures with high or low fluid transmissivity and it is not possible to estimate the lateral extent of the fractures. Some of the fracturelike features seen in the logs could be drilling induced and thus not extend far from the borehole. Pressure transient tests can give an estimate of fluid transmissivity of fractures, but these are macroscopic measurements averaging over a large conducting region.

On a reservoir scale, seismic methods are at the forefront for detecting and analyzing fracture networks. The scale of a fracture relative to the seismic wavelength determines the nature of the fracture signature in the wavefield (Fang et al., 2012). Microfractures or cracks that are much smaller than the seismic wavelength are known to cause velocity anisotropy. Considerable research has been done to characterize microfractures through effective medium theories (e.g., Peacock and Hudson, 1990; Kachanov, 1992). It is common to apply methods such as amplitude variation with offset and azimuth (AVOA) to characterize the velocity anisotropy that can be interpreted to characterize the preferred orientation of the fractures. It is not possible to independently estimate the fracture spacing and fracture transmissivity using AVOA analysis. The focus now is increasingly on detecting large discrete fractures that have a larger impact on fluid flow. These macrofractures have a lateral extent comparable to the wavelength of the incident wavefield (tens of meters) and the spacing between these fractures or fracture zones may be on the order of a wavelength. Such fractures can scatter the seismic wavefield (Willis et al., 2006; Burns et al., 2007). They are treated as distinct features rather than as an effective medium. Descriptive distributions of such networks are usually referred to as discrete fracture networks and can be used to stochastically model fluid flow in reservoirs. Willis et al. (2006), Burns et al. (2007), Grandi (2008), and Fang et al. (2012) develop scattering-based

Manuscript received by the Editor 14 December 2012; revised manuscript received 11 March 2013; published online 24 June 2013.
[1]Massachusetts Institute of Technology, Earth Resources Laboratory, Cambridge, Massachusetts, USA. E-mail: sudhi@mit.edu; fehler@mit.edu; burns@mit.edu.

methods to determine fracture orientation and spacing from seismic reflection data. Scattered wave signals are a function of fracture compliance. Grandi (2008) numerically simulates scattering from a parallel set of discrete fractures and shows that the amplitude of the scattered wavefield increases with increasing fracture compliance.

Fracture compliance

Fracture compliance is the inverse of fracture specific stiffness (Pyrak-Nolte et al., 1990) and is defined as the displacement across the fracture surfaces when a unit stress is applied across the fracture. Laboratory studies suggest that fracture compliance and fracture fluid transmissivity are influenced by the same microscopic features of the fracture, i.e., aperture distribution, actual contact area, fractal dimension of the fracture surfaces, and that these are interrelated (Pyrak-Nolte and Morris, 2000). Therefore, fracture compliance may be a key link to estimate fracture fluid transmissivity from scattered energy (Brown and Fang, 2012). Measuring the fracture compliance in a borehole, we may be able to assign fracture compliance and thus, fracture transmissivity, to regions away from the borehole based on relative scattered energy measured on surface seismic data. In addition, estimating fracture compliance in a borehole may be useful for monitoring the efficiency of hydraulic fracturing. Therefore, it is important to understand the range of compliance values that can be expected in the subsurface.

Estimates of fracture compliance vary over orders of magnitude from laboratory to the field. Worthington and Lubbe (2007) suggest that fracture compliance scales with fracture size, which would explain the small compliance value measured in the lab (Pyrak-Nolte et al., 1990; Lubbe et al., 2005) and the scattering effects seen at field seismic wavelength scales. However, compliance measurements in the field are limited and are mostly based on effective medium methods by assuming some fracture density. In this paper, we develop models that estimate fracture compliance, aperture, and size in the field by studying (1) tube-wave generation and (2) tube-wave attenuation at a fracture intersecting a borehole. When an external wavefield is incident on a fluid-filled fracture intersecting a borehole (e.g., VSP), it squeezes the fracture and expels fluid into the borehole, generating a tube wave in the borehole. The amplitude of the tube wave is proportional to the amount of fluid exchanged between the fracture and the borehole. The fluid exchange, in turn, depends on the compliance and fluid transmissivity of the fracture. The amplitude ratio of the pressure due to the incident wavefield measured in the borehole fluid to the pressure due to the tube wave generated at the fracture can be diagnostic of fracture compliance and fracture transmissivity. Similarly, when a borehole tube wave that is generated elsewhere propagates across a fracture, part of its energy is spent in pushing the fluid into the conducting fracture. This energy loss depends on the amount of fluid exchanged, and the attenuation coefficient is a function of the fracture properties.

Tube-wave generation at a fracture is first studied by Beydoun et al. (1985). However, Beydoun does not consider fracture compliance. Later, Hardin et al. (1987) formulate fracture closure as a function of fracture compliance. Beydoun and Hardin assume Darcy flow in the fracture, which is a low-frequency approximation to the dispersion relation in the fracture (Tang, 1990). Cicerone and Toksöz (1995) and Ionov (2007) study tube-wave generation by taking the high-frequency approximation solution to the dispersion relation in the fracture. Though Ionov (2007) does not consider fracture compliance, Cicerone and Toksöz (1995) attempt to include fracture compliance indirectly by allowing displacement to be discontinuous at the fracture top and bottom surfaces.

Attenuation of tube waves across a fracture was studied by Mathieu (1984), Hornby et al. (1989), Tang and Cheng (1993), and Kostek et al. (1998a, 1998b). Mathieu (1984) assumes Darcy flow in the fracture and studies attenuation of tube waves across the fracture. However, the assumption of Darcy flow is not valid for typical logging frequencies. Hornby et al. (1989) and Tang and Cheng (1993) solve the problem under a high-frequency approximation, which is a valid assumption for acoustic logging (kHz range of frequencies) and fractures like those expected in situ. Later, Kostek et al. (1998b) extend the theory to include the elasticity of the formation. These studies do not account for the fracture compliance that play an important role in the tube-wave attenuation.

In this paper, we develop models for tube-wave generation and attenuation that account for fracture compliance and are valid over a broad range of frequencies (Hz to kHz). To study tube-wave generation and attenuation at arbitrary frequency, we numerically solve for the dispersion relation in the fracture. We first describe the models for an infinitely long fracture to understand the affects of fracture aperture and fracture compliance. The models predict a low-frequency regime, a high-frequency regime, and a transition regime in which the viscous skin depth is comparable to the fracture aperture. Based on these observations, we show that measurements in the transition regime are required to infer fracture aperture and compliance. However, we discuss how data collected in the high-frequency regime can be used to place a lower bound on fracture compliance. We then extend the models to the finite fracture case and discuss the affect of the finite length of fracture. Finite fracture models are described in Appendices A and B. Finally, we present a field data example to argue that fracture compliance of the order of 10^{-9} is feasible in the field.

THEORETICAL FORMULATION

Tube-wave generation in a borehole

Following previous studies, we consider a horizontal fracture that is infinite in lateral extent and intersecting a vertical borehole of radius R as shown in Figure 1. The model is developed to study the tube-wave generation in the borehole when a plane P-wave is normally incident on the fracture. However, the results can be extended to an arbitrary angle of incidence. Fractures are discontinuities in the subsurface, held open by asperities that resist the fracture closure. For simplicity, we assume the fracture to be a parallel plate with static aperture L_0 and normal compliance, Z. For now, we neglect the effect of roughness, tortuosity, and actual contact area of the fracture on the fluid motion in the fracture; however, these will be discussed in a later section. Fracture closure is proportional to the compliance and the applied effective normal stress. Though fracture closure and applied stress are nonlinearly related (Pyrak-Nolte et al., 1990), fracture closure due to the perturbation in the applied stress over a background lithostatic stress due to an incident wavefield can be considered locally linear (Schoenberg, 1980). Therefore, the dynamic fracture $L(t)$ aperture at any location can be written as (Hardin et al., 1987)

$$L(t) = L_0 + Z[p(t) - \sigma_n(t)], \tag{1}$$

where L_0 is the static aperture, $\sigma_n(t)$ is the normal stress on the fracture face, and $p(t)$ is the perturbation in the fracture fluid pressure due to closure.

For a normally incident P-wave, $\sigma_n(t) = \sigma_0 e^{-i\omega t}$, where σ_0, ω are the stress amplitude and frequency of the incident wave. The incident wave perturbs the fracture aperture and causes a pressure gradient in the fracture. For simplicity, fluid pressure and flow in the fracture are averaged over the aperture and only their radial variation away from the borehole is considered. We use cylindrical coordinates to accommodate the axial symmetry of the problem. The net flow out of a volume element $2\pi r L(t)\, dr$ between r and $r + dr$ from the axis of the borehole, during a time increment dt, should equal the change in volume of the element due to the perturbation in the aperture and the change in the fluid volume due to compressibility of the fluid. Thus, we arrive at the mass conservation equation in the fracture as

$$-\left(\frac{\partial q}{\partial r} + \frac{q}{r}\right) = \frac{dL}{dt} + L\gamma\frac{\partial p}{\partial t}, \tag{2}$$

where γ is the fluid compressibility and q is the radial flow per unit length away from the borehole. Flow in the fracture can be related to the pressure gradient through dynamic conductivity $\bar{C}$. Solving for the flow field of a viscous fluid in an infinitely long rigid fracture, Tang (1990) shows that the flow averaged over the aperture at any location could be related to the radial pressure gradient at that location as

$$\bar{q} = -\bar{C}\frac{\partial \bar{p}}{\partial r} = -\frac{i\omega L_0}{k_r^2 \alpha_f^2 \rho_f}\frac{\partial \bar{p}}{\partial r}, \tag{3}$$

where α_f is the acoustic velocity in the fluid, ρ_f is the fluid density, and i is the imaginary unit. A bar over a symbol denotes that the quantity is in the frequency domain. The radial wavenumber of those specific modes that can exist in a rigid fracture (zero fracture compliance) is represented by k_r and is obtained by solving the dispersion relation for the velocity field in an infinitely long, fluid-filled fracture, given by (Tang, 1990)

$$k_r^2 \tan\left(\frac{\eta_2 L_0}{2}\right) + \eta_1\eta_2 \tan\left(\frac{\eta_2 L_0}{2}\right) = 0, \tag{4a}$$

$$\eta_1^2 + k_r^2 = \frac{\omega^2}{\alpha_f^2 - \frac{4}{3} i\omega\nu}, \tag{4b}$$

$$\eta_2^2 + k_r^2 = \frac{i\omega}{\nu}, \tag{4c}$$

where ν is the kinematic viscosity of the fluid. Given the small strains associated with exploration seismic waves, and for the range of the fracture apertures and the fracture compliances that are practical, fracture closure is small compared to the fracture aperture. So, we approximate the modes in the fracture with that of a rigid fracture given by Tang's (1990) dispersion relationship. The effect of fracture compliance is taken into account in equation 2. Thus, inserting equation 3 for radial flow and equation 1 for the dynamic aperture into the mass conservation equation 2 and neglecting higher order terms, we can write the frequency domain differential equation for fluid pressure in the fracture as

$$\frac{\partial^2 \bar{p}}{\partial r^2} + \frac{1}{r}\frac{\partial \bar{p}}{\partial r} + \zeta^2 \bar{p} = \sigma_0 \frac{\rho_f Z \zeta^2 \alpha_{eff}^2}{L_0}, \tag{5}$$

where $\zeta = k_r \alpha_f/\alpha_{\text{eff}}$, $1/\alpha_{\text{eff}}^2 = 1/\alpha_f^2 + \rho_f Z/L_0$, ζ is the wavenumber for the pressure field in a compliant fracture, and α_{eff} is the propagation velocity of the pressure field at the high-frequency limit. As $r \to \infty$, flow in the radial direction tends to zero and we require that $\partial\bar{p}/\partial r = 0$. At the borehole wall, we require that the fluid pressure in the fracture $\bar{p}(\omega)|_{r=R}$ be equal to the fluid pressure due to the tube wave generated in the borehole $\bar{p}_t(\omega)$. The homogeneous solutions to equation 5 are Hankel functions of the first and second kind taking complex arguments. However, the Hankel function of the second kind diverges as $r \to \infty$, while the first kind approaches zero. Taking Hankel functions of the first kind and satisfying the boundary condition at the borehole, the pressure in the fracture can be written as

$$\bar{p}(\omega, r) = \left[\bar{p}_t(\omega) - \frac{\rho_f Z \alpha_{\text{eff}}^2}{L_0}\sigma_0\right]\frac{H_0^1(\zeta r)}{H_0^1(\zeta R)} + \frac{\rho_f Z \alpha_{\text{eff}}^2}{L_0}\sigma_0, \tag{6}$$

where H_m^n is the Hankel function of the nth kind and order m.

The pressure in the fracture, given by equation 6 satisfies the wave equation when ζ^2 and k_r^2 are real and it follows a diffusion equation when ζ^2 and k_r^2 are imaginary. Tang (1990) solves the dispersion relation at high- and low-frequency limits and shows that k_r^2 is real at the high-frequency limit and is imaginary at the low-frequency limit. At the high-frequency limit, the fracture aperture is much greater than the viscous skin depth, $\delta = \sqrt{2\nu/\omega}$, and the inertial forces dominate. At the low-frequency limit, the fracture aperture is much smaller than the viscous skin depth and the viscous forces dominate. For $\nu = 10^{-6}$ m^2/s (value typical for water) and for the range of natural fracture apertures (0.1–1 mm), δ/L_0 varies from 0.07 to 1.78 over the typical VSP frequency band of 10–60 Hz. Hence, either the high- ($\delta/L_0 \ll 1$) or low-frequency ($\delta/L_0 \gg 1$) approximation is not valid. In this transition zone, k_r^2 is complex and the pressure field has propagative and dispersive components. To address this, for an arbitrary frequency, we solved the dispersion relation, equation 4, numerically for k_r^2. The dispersion relation is nonlinear and has an infinite number of solutions corresponding to higher modes. Because the contribution to flow from the higher modes is negligible, we use the fundamental mode solution for k_r^2. Taking the numerical solution for k_r^2, equation 6

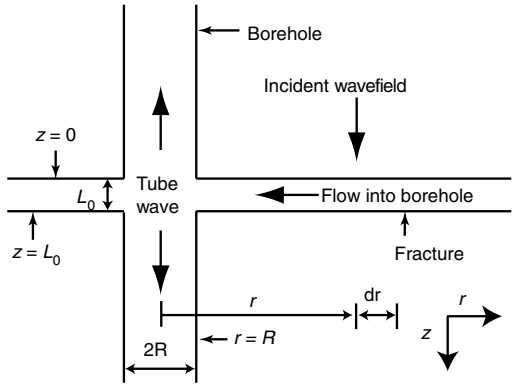

Figure 1. Diagram showing tube-wave generation at a fracture intersecting a borehole.

encapsulates diffusion and wave propagation. Because ζ is complex, the propagation velocity of the pressure field is given by $\omega/\mathcal{R}_e\{\zeta\}$ and the attenuation factor is given by $\mathcal{I}_m\{\zeta\}$. The dispersion relation for the propagation velocity for different fracture compliance values and apertures is shown in Figure 2. The propagation velocity approaches zero toward low frequencies, as the pressure field is more diffusive. At the high-frequency limit, the propagation velocity approaches α_{eff} and for a rigid fracture, the propagation velocity approaches the speed of sound in the fluid. Note that the propagation velocity decreases with increasing compliance and decreasing aperture. This is analogous to a pressure pulse propagating in an elastic tube. The speed of the pulse decreases, as the tube is more elastic. Figure 3 shows the attenuation factor as a function of frequency. As expected, higher frequencies attenuate more. As the aperture decreases, viscous forces dominate and attenuation increases. As compliance increases, the propagation velocity decreases and the pressure pulse attenuates more in the same travel distance.

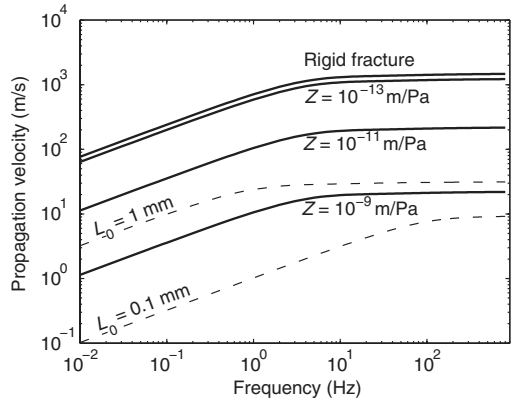

Figure 2. Propagation velocity for fluid pressure in the radial direction in a fracture $\omega/\mathcal{R}_e\{\zeta\}$ is plotted against frequency for different values of compliance and aperture. The solid lines represent varying compliance when fracture aperture is 0.5 mm. The dotted lines represent varying fracture aperture when fracture compliance is 10^{-9} m/Pa. The propagation velocity is obtained by numerically solving Tang's dispersion relation using the following: $\alpha_f = 1500$ m/s, $\alpha = 5800$ m/s, $\beta = 3300$ m/s, $\rho_f = 1000$ kg/m^3, $\rho = 2700$ kg/m^3, and $\nu = 10^{-6}$ m^2/s. The fluid properties correspond to water.

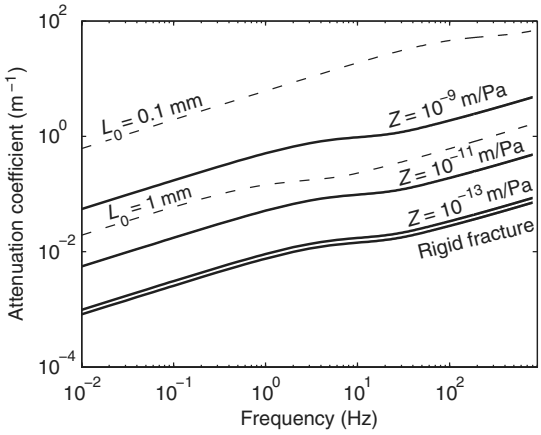

Figure 3. Attenuation factor $\mathcal{I}_m\{\zeta\}$ for fluid pressure in a fracture is plotted against frequency for different values of compliance and aperture. The solid lines represent varying compliance when the fracture aperture is 0.5 mm. The dotted lines represent varying fracture aperture when fracture compliance is 10^{-9} m/Pa. The parameters for this study are the same as in Figure 2.

We now proceed to estimate the amplitude of tube wave generated in the borehole. Knowing the distribution of pressure in the fracture from equation 6, the pressure gradient at the borehole wall and thus the flow into the borehole can be estimated from equation 3. The rate of volume injection into the borehole dV/dt is equal to the volume of fluid flowing from the fracture into the borehole per unit time and is given by

$$\frac{dV}{dt} = -2\pi R q|_{r=R}. \tag{7}$$

Because q denotes fluid flowing away from the origin, the negative sign is needed for fluid flow into the borehole. This fluid exchange between the fracture and the borehole acts as a volume source and generates a tube wave of amplitude p_t given by (Lee and Balch, 1982)

$$p_t = \frac{\rho_f c_t}{2\pi R^2}\frac{dV}{dt}, \tag{8}$$

where $c_t = \alpha_f/\sqrt{1+\rho_f\alpha_f^2/(\rho_s\beta^2)}$ (White, 1983), is the tube-wave velocity in the borehole and ρ_s, β are the density and shear wave velocity of the formation, respectively. Tube-wave velocity is very weakly dispersive over the frequency range of interest (Hz to kHz) (Cheng and Toksöz, 1982) and thus, taking the low-frequency approximation solution given by White (1983) does not affect subsequent analysis. Eliminating the rate of fluid injection from equations 7 and 8 and using equations 3 and 6, we arrive at the expression for an equivalent pressure source for the tube wave in the frequency domain as

$$\bar{p}_t(\omega) = \sigma_0 \frac{\omega}{k_r\alpha_f}\frac{c_t}{\alpha_{\text{eff}}}\frac{L_0}{R}\frac{p_f\alpha_{\text{eff}}^2}{L_0/Z} \times \left[\frac{iH_1^1(\zeta R)/H_0^1(\zeta R)}{1+\frac{\omega}{k_r\alpha_f}\frac{c_t}{\alpha_{\text{eff}}}\frac{L_0}{R}iH_1^1(\zeta R)/H_0^1(\zeta R)}\right]. \tag{9}$$

At the same time, the incident P-wave traveling along the borehole induces dynamic pressure in the borehole given by (White, 1983)

$$\bar{p}_i(\omega) = \sigma_0\frac{\rho_f c_t^2}{\rho_s\beta^2}\left(\frac{1-2\beta^2/\alpha^2}{1-c_t^2/\alpha^2}\right). \tag{10}$$

By taking the pressure amplitude ratio $\bar{p}_t/\bar{p}_i$, we eliminate σ_0. Figure 4 shows the amplitude ratio plotted against frequency for a given fracture compliance and aperture. For comparison, the amplitude ratios found using the low- and high-frequency approximation solutions to the dispersion relation in the fracture are plotted as well. At the low-frequency limit, the amplitude ratio tends toward zero. With increasing frequency, the amplitude ratio increases and reaches a maximum at the transition from low- to high-frequency regimes and then decreases with further increase in frequency. However, at a high frequency, the amplitude ratio reaches a constant

value roughly proportional to $\sqrt{ZL_0}$. Over the entire frequency range, the amplitude ratio increases with fracture compliance (see Figure 5). It is easier to squeeze more fluid into the borehole because the fracture is more compliant. However, the location of the peak in the amplitude ratio is independent of the fracture compliance. The peak occurs at the transition from the low- to high-frequency limit and depends on the fracture aperture and the viscosity of the fluid. For larger apertures, the peak occurs at lower frequencies (see Figure 6), and for higher viscosities, the peak occurs at higher frequencies (see Figure 7). Thus, the location of the peak can be indicative of the fracture aperture, and the amplitude ratio can be indicative of fracture compliance.

Tube-wave generation at a finite fracture

The amplitude ratio for a finite-length fracture is derived in Appendix A. Figure 8 shows the amplitude ratio plotted for varying fracture lengths. The effect of the finite length of a fracture is that the wave reflects at the fracture tip. As a result, the amplitude ratio is amplified at those frequencies that interfere constructively and attenuated at those frequencies that interfere destructively. This results in a series of peaks and troughs overlaid on the infinite fracture response. Higher frequencies attenuate more (see Figure 3) over the same fracture length, and as a result the peaks/troughs reduce in amplitude with increasing frequency. As shown in Appendix A, frequencies greater than $\omega_d = 5.3(\alpha_{\text{eff}} L_0/\delta(D-R))$ are insensitive to the finite extent of the fracture and the amplitude ratio matches with that of an infinitely long fracture. This frequency ω_d can be suggestive of fracture length. The spacing between consecutive peaks or troughs in the amplitude ratio varies with frequency and is dependent on the fracture compliance, fracture aperture, and the length of the fracture. However, under the high-frequency approximation, the spacing between consecutive peaks or troughs Δ (in Hz) is constant and relates fracture length to aperture and compliance through (see Appendix A): $\Delta = \alpha_{\text{eff}}/2(D-R)$.

Tube-wave attenuation in a borehole

We next consider tube-wave attenuation across an infinitely long horizontal fracture intersecting a borehole. Figure 9 shows a schematic diagram of tube-wave attenuation. The geometry is the same as that described for tube-wave generation in the previous section. When a tube wave crosses a fracture intersecting the borehole, part of its energy is spent in pushing the fluid into the fracture and part of the energy is reflected at the interface. As a result the transmitted wave is attenuated. The attenuation of the tube wave depends on the amount of fluid pushed into the fracture, which in turn depends on the fracture transmissivity and compliance. Considering the continuity of the pressure field in the borehole at the fracture top ($z = 0$) and, applying mass conservation in the borehole while accounting for the flow into the fracture, Mathieu (1984) obtains the transmission coefficient as

$$\frac{\bar{p}_{tt}}{\bar{p}_{ti}} = \frac{1}{1 + \frac{fL_0}{2}\frac{I_0(fR)}{I_1(fR)}\frac{\rho_f c_t}{Z_F}}, \tag{11a}$$

$$f = \frac{\omega}{c_i}\sqrt{1 - \frac{c_t^2}{\alpha_f^2}}, \tag{11b}$$

where f is the radial wavenumber of the tube waves in the borehole; Z_F is the fracture acoustic impedance, defined as the ratio of average pressure to average fluid velocity across the fracture at the borehole wall; and I_m is the modified Bessel function of the first kind of order m. Because the wavelength of the tube wave is larger than the borehole radius and the fracture aperture, the pressure in the borehole is assumed to be constant over the borehole radius and over the fracture aperture. Mathieu (1984) obtains Z_F by assuming Darcy flow in the fracture, a low-frequency approximation, and did not consider the effect of the fracture compliance. The dynamic aperture of the compliant fracture, in our model, is given by equation 1. However, we take $\sigma_n(t)$ to be zero, because we do not have an external wavefield that is incident on the fracture in the tube-wave attenuation model. The differential equation for the pressure field in the fracture $\bar{p}$ is obtained by following the same steps as described in the tube-wave generation model and is given by

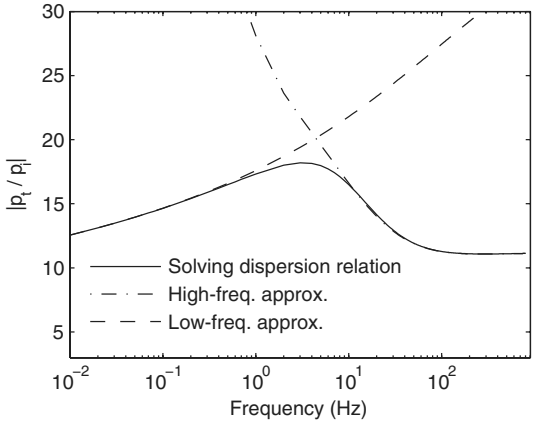

Figure 4. Tube to P-wave pressure amplitude ratio is plotted against frequency for a 0.5-mm-wide fracture with a fracture compliance of 10^{-9} Pa/m, intersecting a 15-cm diameter borehole. The formation and fluid properties are the same as in Figure 2.

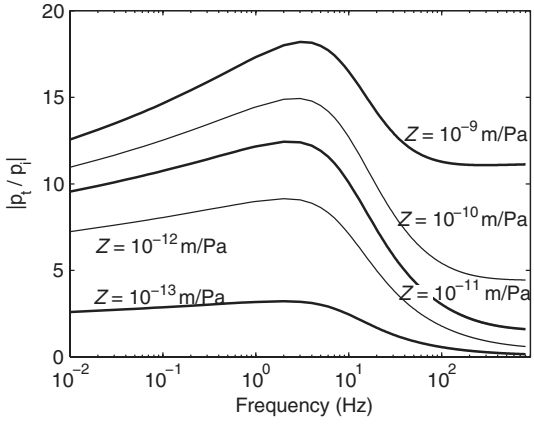

Figure 5. Tube to P-wave pressure amplitude ratio plotted against frequency for different fracture compliance values, taking $L_0 =$ 0.5 mm, while other parameters are kept constant. Note that the amplitude ratio decreases with decreasing compliance and the transition regime is independent of compliance. The parameters for this study are the same as in Figure 4.

$$\frac{\partial^2 \bar{p}}{\partial r^2} + \frac{1}{r}\frac{\partial \bar{p}}{\partial r} + \zeta^2 \bar{p} = 0 \tag{12}$$

with the following boundary conditions: (1) At the borehole wall, the pressure in the fracture should be equal to that of the transmitted tube wave; i.e., $\bar{p}(R) = \bar{p}_{tt}(R)$. Here, we assume that the pressure due to the transmitted wave in the borehole drives the flow into the fracture. (2) Flow in the radial direction tends to zero at infinity, and we require that $\partial \bar{p}/\partial r = 0$, as $r \to \infty$. Solving equation 12, the pressure in the fracture can be written as

$$\bar{p}(r) = \bar{p}_{tt}\frac{H_0^1(\zeta r)}{H_0^1(\zeta R)}. \tag{13}$$

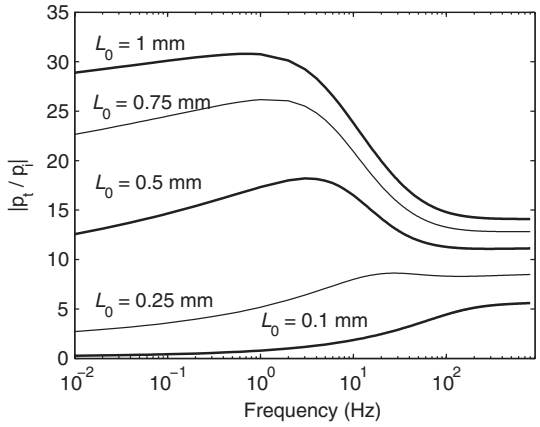

Figure 6. Tube to P-wave pressure amplitude ratios are plotted against frequency for different values of aperture, taking $Z = 10^{-9}$ m/Pa, while other parameters are kept constant. Note that the transition regime moves toward higher frequencies with decreasing aperture. Also, the amplitude ratio decreases with the decreasing aperture. Medium parameters are the same as in Figure 4.

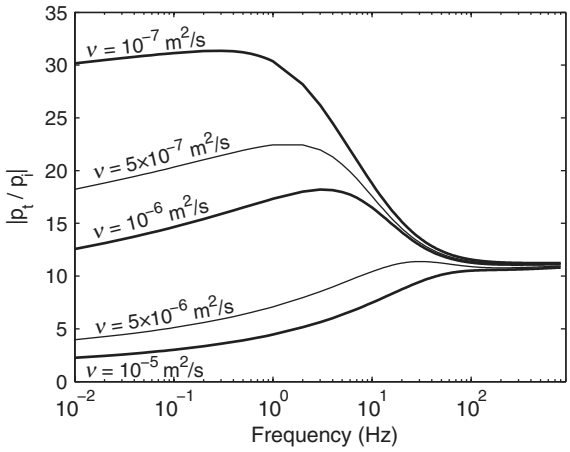

Figure 7. Tube to P-wave pressure amplitude ratios plotted against frequency for different kinematic viscosity values, taking $Z = 10^{-9}$ m/Pa and $L_0 = 0.5$ mm, while other parameters are kept constant. Note that the transition regime moves toward higher frequencies with increasing viscosity. The parameters other than viscosity are the same as in Figure 4.

Knowing the distribution of pressure in the fracture from equation 13 and using equation 3, the radial flow into the fracture is given by

$$\bar{q}(R) = \bar{p}_{tt}\zeta\frac{i\omega L_0}{k_r^2\alpha_f^2\rho_f}\frac{H_1^1(\zeta R)}{H_0^1(\zeta R)}. \tag{14}$$

Thus, the impedance of the fracture can be written as

$$Z_F = \frac{<\bar{p}(R)>}{<\bar{v}_F(R)>} = \frac{\bar{p}_{tt}}{\bar{q}(R)/L_0}, \tag{15a}$$

$$= \frac{k_r^2\alpha_f^2\rho_f}{i\omega\zeta}\frac{H_0^1(\zeta R)}{H_1^1(\zeta R)}. \tag{15b}$$

Inserting Z_F from equations 15 into equation 11, the transmission coefficient can be estimated. Taking $\zeta = k_r = \omega/\alpha_f$, equation 15 matches the solutions given by Hornby et al. (1989) and Tang and Cheng (1993) for a rigid fracture ($Z = 0$), at the high-frequency limit. The transmission coefficient, for an infinitely long fracture, is plotted against frequency for a given compliance and aperture in Figure 10. For comparison, the transmission coefficients under the low- and high-frequency approximations are plotted as well. At the low-frequency limit, $(H_1^1(\zeta R))/(H_0^1(\zeta R))$ approaches zero and the transmission coefficient tends toward unity. In contrast, Hornby (1989) predicts that the transmission coefficient goes to zero toward low frequencies, consistent with the high-frequency limit solution (see Figure 10). However, his solution does not account for viscosity, which dominates at lower frequencies. The transmission coefficient shows a transition from low to high frequency, similar to the tube-wave generation model. With increasing frequency, the transmission coefficient decreases and reaches a minimum at the transition from low- to high-frequency and then increases with further increase in frequency. However, in the high-frequency regime, the transmission coefficient reaches a constant value. In general, as compliance increases, the transmission coefficient decreases over the entire frequency band (see Figure 11). Thus, a compliant fracture can explain low transmission coefficients observed in the field without demanding excessively high apertures, which is the case when fracture compliance is not considered (Hornby et al., 1989). For a given compliance, the location of the frequency having the minimum in the transmission coefficient depends on the viscosity of the fluid and the fracture aperture. Increasing viscosity pushes the minimum toward higher frequencies and larger aperture moves the minimum toward lower frequencies (see Figures 12 and 13). This dependence of transition regime frequency on compliance, aperture, and viscosity is the same as seen for tube-wave generation from an incident P-wave in the previous sections.

Tube-wave attenuation at a finite fracture

Fracture impedance for a finite-length fracture is derived in Appendix B. Figure 14 shows transmission coefficients for a finite fracture case. The effect of the finite length of the fracture is to cause peaks/troughs overlaid on the infinite fracture response, similar to the tube-wave generation model. The decay of the peaks/troughs

and the spacing between consecutive peaks/troughs at high frequencies are suggestive of the fracture length for the same reasons discussed in the tube-wave generation section. We find that the expressions for the frequency, ω_d, at which the finite fracture response matches the infinite fracture response, and the spacing between consecutive peaks/troughs at high frequencies, Δ, are the same as that for the tube-wave generation model and are derived in Appendices A and B.

Effect of dynamic tortuosity and permeability

Real fractures are rough surfaces in contact (Brown and Scholz, 1985) and are rarely parallel plates, as idealized in the models discussed in this paper. In a fracture, aperture is spatially varying and it is zero at the asperities, where the fracture surfaces are in contact. At a microscopic level, fractures are similar to porous media. Johnson et al. (1987) describe wave propagation in a porous medium in terms of dynamic tortuosity Ω and dynamic permeability K given by

$$\Omega = \Omega_\infty + \frac{i\mu\phi}{\omega K_0 \rho_f} F(\omega), \tag{16a}$$

$$K = \frac{i\mu\phi}{\Omega\omega\rho_f}, \tag{16b}$$

where ϕ is the porosity, Ω_∞ is the real valued tortuosity at infinite frequency, K_0 is the real valued permeability at zero frequency, and $F(\omega)$ is a complex-valued function such that (1) the dynamic tortuosity reduces to Ω_∞ at infinite frequency and (2) the dynamic permeability reduces to K_0 at zero frequency. At frequencies in between, the dynamic tortuosity and dynamic permeability are complex. From equation 16, we can see that dynamic tortuosity and dynamic permeability are related and either can be used to describe wave propagation in porous media. The real part of the dynamic tortuosity reduces the wave propagation velocity. At infinite frequency, the propagation velocity is reduced to $\alpha_f/\sqrt{\Omega_\infty}$ due to tortuosity (Johnson et al., 1987). The imaginary part is related to attenuation and dispersion due to viscous losses. Viscous losses are proportional to the solid-fluid contact area, and it is assumed that parallel plate flow accounts for most of the viscous losses. The parallel plate assumption is well tested in the laboratory and is valid for rough fractures as long as the actual contact area at the asperities is less than 30% of the fracture surface area (Witherspoon et al., 1980; Tsang, 1984). The actual contact area depends on the aperture distribution and normal stress. Laboratory measurements by Bandis et. al (1983) on several granite and limestone samples show that actual contact area is between 40% and 70% for normal stresses above 30 MPa. For fractures with a large actual contact area, the flow is more complicated (Zimmerman and Bodvarsson, 1996) and the flow rate drops by orders of magnitude (Tsang, 1984). Such fractures may not be of practical interest. Moreover, the stress at which the parallel plate assumption breaks down depends on the aperture distribution and may scale up for large discrete fractures that have broader distributions of apertures (Tsang and Witherspoon, 1983). For the current discussion, we assume that the parallel plate law adequately represents the viscous losses. Tang (1990) shows that under the low-frequency approximation, the dynamic permeability estimated from his model approaches that from

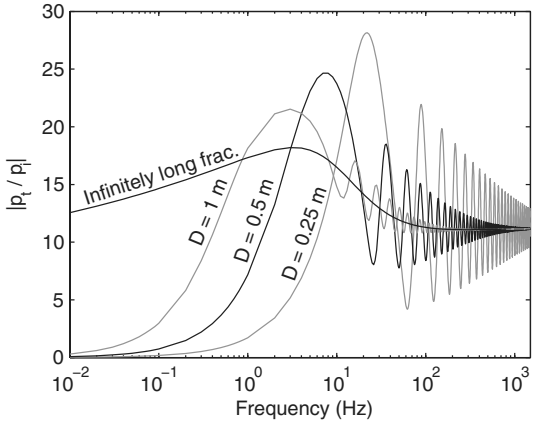

Figure 8. Tube to P-wave pressure amplitude ratio is plotted against frequency for fractures of different fracture lengths, taking $Z = 10^{-9}$ m/Pa and $L_0 = 0.5$ mm, while other parameters are kept constant. All other parameters are the same as in Figure 4.

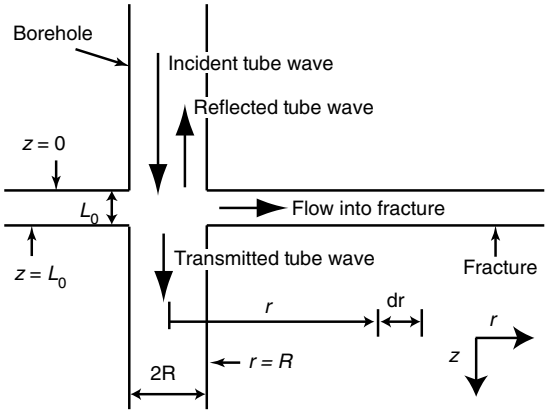

Figure 9. Schematic showing attenuation of a tube wave at a fracture intersecting a borehole.

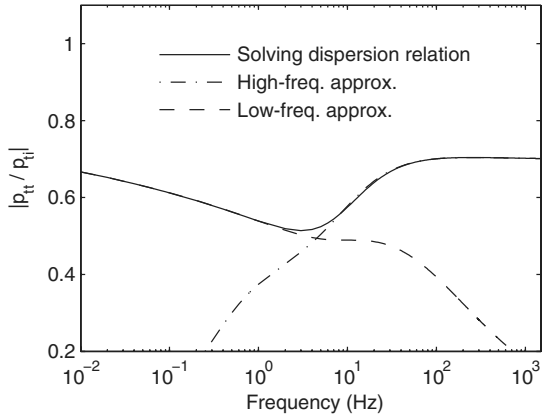

Figure 10. Transmission coefficient is plotted against frequency assuming a fracture compliance of 10^{-9} Pa/m and an aperture of 0.5 mm. The parameters for this study are the same as in Figure 4.

the parallel plate law. Thus, the estimates of the pressure amplitude ratio or the transmission coefficient, at the low-frequency limit, are reliable for fractures with actual contact area less than 30%. However, the dynamic tortuosity estimated from Tang's model approaches one at high frequencies implying no tortuosity. To look at the effect of dynamic tortuosity at the high-frequency limit, we solve the dispersion relation in the fracture by taking the velocity of wave propagation in the fracture fluid to be $\alpha_f/\sqrt{\Omega_\infty}$. As $\omega \to \infty$, k_r is given by $\sqrt{\Omega_\infty}(\omega/\alpha_f)$ and $H_1^1(\zeta R)/H_0^1(\zeta R)$ approaches $-i$. Thus, taking the high-frequency approximation, the amplitude of the generated tube wave, equation 9, and the fracture impedance, equation 15, can be written as

$$\bar{p}_t(\omega) = \sigma_0 \frac{\rho_f c_t Z}{R} \frac{1}{\sqrt{\frac{\Omega_\infty}{\alpha_f^2} + \frac{\rho_f Z}{L_0}}}, \tag{17a}$$

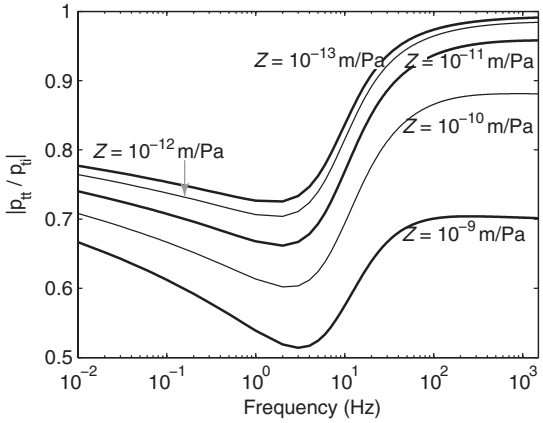

Figure 11. The transmission coefficient is plotted against frequency for different fracture compliance values, taking $L_0 = 0.5$ mm, while other parameters are kept constant. Note that the transmission coefficient increases with decreasing compliance and the transition regime is independent of compliance. The parameters for this study are the same as in Figure 4.

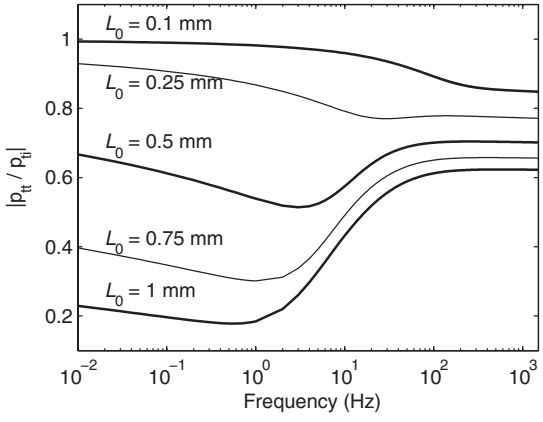

Figure 12. Transmission coefficients are plotted against frequency for different values of aperture, taking $Z = 10^{-9}$ m/Pa, while other parameters are kept constant. Note that the transition regime moves toward higher frequencies with decreasing aperture. Also, the transmission coefficient increases with decreasing aperture. Medium parameters are the same as in Figure 4.

$$Z_F = \rho_f \frac{1}{\sqrt{\frac{\Omega_\infty}{\alpha_f^2} + \frac{\rho_f Z}{L_0}}}. \tag{17b}$$

Johnson et al. (1987) show that the values of Ω_∞ range from one for a parallel plate to three for a typical porous medium; therefore, the value for fractures should lie between one and three. When $(\rho_f Z)/(L_0) \gg (\Omega_\infty)/(\alpha_f^2)$, the effect of tortuosity is negligible on the amplitude ratios and transmission coefficients. This is true for compliance values greater than 10^{-11} m/Pa. When $(\rho_f Z)/(L_0) \ll (\Omega_\infty)/(\alpha_f^2)$, the amplitude ratio and fracture impedance are reduced by a factor of $1/\sqrt{\Omega_\infty}$. In a porous medium, the transition from low to high frequency depends on the viscous skin depth relative to the pore size (Johnson et al., 1987). For fractures, the mean fracture aperture L_0 is a good estimate of the pore size and, thus, the transition frequency is captured well by comparing the viscous skin depth to the parallel plate fracture aperture.

FIELD DATA ANALYSIS

Overview

The magnitude of the amplitude ratio of the generated tube wave to that of the incident P-wave can be easily determined from the power spectra of the VSP data and can be used to invert for fracture properties (Hardin et al., 1987). The waveforms corresponding to the incident wave and the generated tube wave are separated in time on the traces recorded in the borehole as you move away from the fracture. At a receiver far enough from the fracture such that the two waveforms are separated in time, the waveforms are windowed and their amplitude spectra are calculated. The ratio as a function of frequency is measured by taking the ratio of the amplitude spectra at each frequency. We can set up an inverse problem to estimate the aperture and compliance such that the observed amplitude ratio at all the frequencies matches with the tube-wave generation model. If the data span the transition regime, the location of the maximum can be used to first estimate the fracture aperture. The maximum occurs when the viscous skin depth is comparable to the fracture aperture. Viscous skin depth at the frequency corresponding to the maximum in the amplitude ratio is a good estimate of the fracture aperture. Knowing the fracture aperture, fracture compliance can be estimated from the amplitude ratio at high frequencies. Thus, the inverse problem is well constrained when we have data spanning the transition regime. If the amplitude ratio is measured only in the high-frequency regime, different combinations of compliance and aperture can satisfy the high-frequency limit (the flat region of the curve in Figure 4) and data collected in this regime cannot independently constrain compliance and aperture. The inverse problem will be ill constrained if the data are collected only in the high-frequency regime. However, the behavior of the amplitude ratio as a function of compliance and aperture does allow us to place a bound on the fracture compliance value. We varied the aperture values from 0.1 to 1 mm and compliance from 10^{-14} to 10^{-5} m/Pa and plotted contours for constant values of amplitude ratio at a given frequency as shown in Figure 15. We can see that the amplitude ratio flattens after some aperture value (when $\delta \ll L_0$) and is not greatly influenced by the aperture beyond this point. At these large apertures, an observed amplitude ratio corresponds to a single compliance value. However, at smaller apertures, the contours bend toward higher compliance values. To retain the same amplitude ratio

at smaller apertures, the fracture should be more compliant. So, every amplitude ratio corresponds to a minimum compliance, over the range of apertures that are practical. Allowing a large aperture (probably using the apparent aperture measured from FMI log), we can place a minimum bound on the compliance. Of course, it would be best to collect data at frequencies spanning the transition regime to better constrain all fracture parameters. For practical purposes, the transition regime lies between 1 and 30 Hz for water ($\nu = 10^{-6}$ m^2/s and an aperture range of 0.1 to 1 mm) and it increases to 300 Hz for crude oil ($\nu = 10^{-5}$ m^2/s and an aperture range of 0.1 to 1 mm). Crude oil is more viscous. So the transition regime shifts to higher frequencies.

Amplitude ratios from real data may have multiple peaks/troughs due to the finite extent of the fractures. However, because we showed that these peaks/troughs are superimposed on the infinite fracture response, we can take a moving average of the amplitude ratio data and analyze it using an infinite fracture model to obtain fracture aperture and compliance. Knowing fracture aperture and compliance, we can simulate the amplitude ratio for the infinite fracture case and compare it to the unsmoothed data. If the peaks and troughs can be resolved in the data, we can measure the spacing between consecutive peaks/troughs, Δ, to estimate the fracture length based on equation A-6. Also, we can locate the frequency ω_d at which the amplitudes of these peaks/troughs decay to the infinite fracture response to estimate fracture length by using equation A-7. When the data are collected in the high-frequency regime, we can only place a lower bound on the fracture compliance and then, equation A-6 or A-7 can only be used to obtain a lower bound on fracture length. However, we observe that a fracture that is tens of meters long appears to be an infinite fracture for tube-wave generation or attenuation, and, thus, we may not be able to characterize the length of hydraulic fractures by analyzing the modes that travel through the fracture fluid.

The discussion above is equally valid for obtaining fracture parameters from tube-wave attenuation data. Typical well-log data are generally in the kHz-frequency range and perhaps as low as 500 Hz. Thus, well-log data are in the high-frequency regime and we will not be able to independently measure fracture aperture and compliance. We may be able to analyze the attenuation of tube waves that are excited in the borehole in a VSP setting. Alternatively, microseismic events accompanying hydraulic fracturing are reported to have a dominant frequency band ranging from 200 to 1 kHz (Warpinski, 2009) and occasionally as low as 30 Hz (Fehler and Phillips, 1991). Similarly, microseismic events generated during production are reported to have a frequency band of 10–50 Hz (Kiselevitch, 1991). We propose that analyzing the amplitude ratio of tube waves generated at a fracture during microseismic events and measuring the attenuation of these tube waves as they cross other fractures intersecting the borehole can be useful to characterize the fractures. This methodology may also be applied to evaluate the performance of hydraulic fracturing procedures.

Field example

Hardin et al. (1987) report amplitude ratios from a field VSP experiment at a well in Mirror Lake, New Hampshire. The Mirror Lake borehole was drilled to a depth of about 225 m with a diameter of 0.15 m in a metamorphic sequence of schist and gneiss, intruded by thick, irregular veins of quartz monzonite. Standard wireline logs, full-wave acoustic log (2–20 kHz), and hydrophone VSP (10–1000 Hz) data were collected. The VSP data were bandpass filtered, and the tube-wave to P-wave amplitude ratio was estimated over the frequency range 100–300 Hz. The amplitude ratios, at a frequency of 150 Hz (source band center frequency), corresponding to a fracture at 45 m depth, ranged from 10 to 15. Comparing the observed amplitude ratio to amplitude ratio contours (at 150 Hz) from a model with parameters appropriate for the field study, the lower bound on compliance was found to lie between 3×10^{-10} and 10^{-9} m/Pa (see Figure 15). However, analyzing the same data, Hardin et al. (1987) suggest that compliance values should be of the order of 10^{-12} to 10^{-13} m/Pa. While relating radial flow to the pressure gradient in the fracture, Hardin used Darcy's law applied to parallel plates. This corresponds to the low-frequency approximation of Tang's dynamic conductivity equation 3. Thus, Hardin applies a model valid for the low-frequency regime to data from the high-frequency regime and thus underestimates the fracture compliance. We also analyzed amplitude ratios corresponding to a fracture at 290-m depth in a water well at Hamilton, Massachusetts, drilled

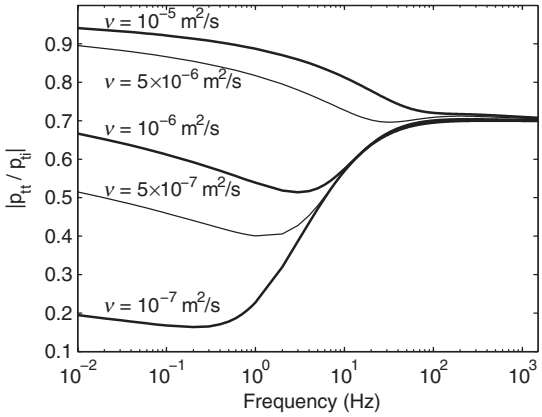

Figure 13. The transmission coefficient is plotted against frequency for different kinematic viscosity values, taking $Z = 10^{-9}$ m/Pa and $L_0 = 0.5$ mm, while other parameters are kept constant. Note that the transition regime moves toward higher frequencies with increasing viscosity. The parameters other than viscosity are the same as in Figure 4.

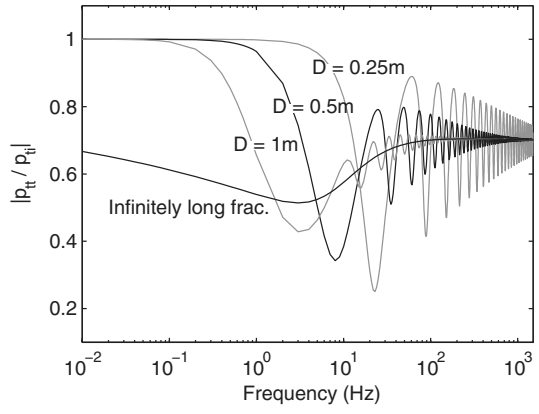

Figure 14. Transmission coefficient is plotted against frequency for fractures of different sizes, taking $Z = 10^{-9}$ m/Pa and $L_0 = 0.5$ mm, while other parameters are the same as in Figure 4.

in a gabbro-granodiorite formation (Hardin, 1986). We find that the lower bound on compliance for this fracture is between 10^{-10} and 10^{-9} m/Pa.

Discussion

It should be noted that the tube-wave generation model is developed for a normal incidence wave on a fracture that intersects the borehole at a right angle, e.g., a vertical borehole and horizontal fracture. However, with increasing depth, fractures are more inclined and tend to be subvertical. Moreover, the incident wavefield may not be parallel to the borehole. When a wave is incident at an angle to the borehole, the pressure amplitude of that wave measured in the borehole increases compared to that of a wave propagating parallel to the borehole (White, 1983). At the same time, nonnormal incidence on a fracture reduces the normal stress on the fracture and decreases the pressure amplitude of the generated tube wave in the borehole. As a result, any deviation from the assumed geometry in the field would mean reduced amplitude ratios and, therefore, fractures of a given compliance will be harder to observe. In other words, an inclined fracture must be more compliant than a horizontal fracture for the same amplitude ratio. Hence, the lower bound on fracture compliance estimated by assuming a horizontally intersecting fracture and normal incidence on the fracture still serves as a lower bound. In addition, the effect of asperities and tortuosity on flow would be to reduce the pressure amplitude ratios. So, the lower bound on fracture compliance from our model is conservative.

The estimate of the lower bound on fracture compliance (on the order of 10^{-10} m/Pa) for the meter-scale fractures in the Mirror Lake experiment is orders of magnitudes larger than the fracture compliance from laboratory measurements and supports the scaling of fracture compliance with fracture length (Worthington et al., 2007). Higher compliance values at larger scales are not surprising. Brown and Scholz (1985) analyze the natural rock surfaces and find that the profiles are fractal and the spatial frequencies have a red-noise power spectrum. Other authors (Hakami and Larsson, 1996) report that apertures are normally distributed. This means that larger apertures are few and spread out spatially at larger distances. When a wave is incident on a fracture, it samples regions on the order of its wavelength. Larger wavelengths sample larger fracture surface and sample larger apertures. A few large apertures can drastically increase the compliance and also increase fluid transmissivity. However, Brown and Scholz (1985) also suggest that fracture surfaces should be correlated after a certain scale. In such a case, we will see an increase in compliance with scale until we reach the correlation length. Although we predict high compliance values (of the order of 10^{-10} m/Pa), one should be careful when applying them to numerical modeling of wave propagation using a linear-slip model (Schoenberg, 1980). A fluid-filled fracture may have compliance similar to a dry fracture under drained conditions, but it becomes much stiffer due to the incompressibility of the fluid under undrained conditions. The overall compliance could also be frequency dependent due to fluid motion, depending on the drainage length compared to the wavelength.

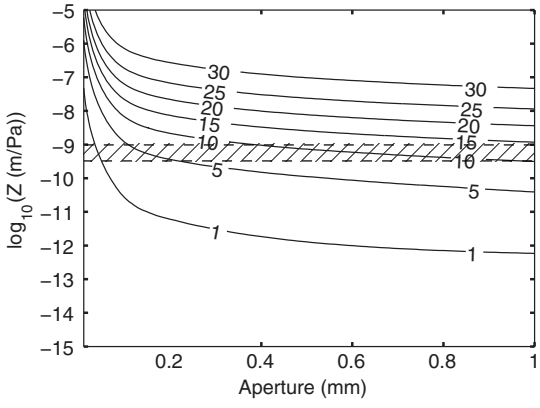

Figure 15. Amplitude ratio contours are plotted in the aperture compliance parameter space for a frequency of 150 Hz. The parameters for the study are the same as in Figure 2 and correspond to the field study at the Mirror Lake borehole (Hardin et al., 1987) discussed in the field example section. Amplitude ratios estimated from the field data lie between 10 and 15. This suggests that the lower bound on the compliance lies between 3×10^{10} and 10^{-9} m/Pa (indicated by the black dotted lines) when the fracture aperture is assumed to be lower than 1 mm.

CONCLUSIONS

Tube-wave generation and attenuation at a fracture intersecting a borehole is modeled accounting for the intrinsic fracture compliance. The pressure field in the fracture was solved without any low/high approximations on frequency. Thus, amplitude ratios and tube-wave attenuation over a range of frequencies and fracture compliances were analyzed. The amplitude ratio/transmission coefficient has a maximum/minimum at a transition frequency. The models suggest that measurements taken near the transition frequency can constrain fracture compliance and aperture more effectively. A finite-length fracture manifests peaks/troughs superimposed the infinite fracture response. If we can resolve the spacing between consecutive peaks/troughs or the decay of the peaks/troughs, we can estimate the fracture length knowing the fracture aperture and fracture compliance. When we have only a minimum bound on the fracture compliance, we can place a minimum bound on the fracture length. Comparing the tube-wave generation model to previously published VSP data suggests that fracture compliance values of the order of 10^{-10} to 10^{-9} m/Pa can be expected in the field. With these values, scattering of seismic waves from such fractured regions should be observed using surface seismic data.

ACKNOWLEDGMENTS

We thank N. Toksöz, A. Malcolm, S. Brown, Y. Zheng, and X. Fang for constructive suggestions and valuable discussions. This work was funded by the Eni Multiscale Reservoir Science Project within the Eni-MIT Energy Initiative Founding Member Program.

APPENDIX A

TUBE-WAVE GENERATION AT A FINITE FRACTURE

The theory described for an infinitely long fracture can be extended to a finite fracture. We consider a penny-shaped horizontal fracture of diameter $2D$ intersecting a borehole at its center. In this case, the differential equation for fluid pressure in the fracture is still given by equation 5. For a finite fracture, we require the zero flow

boundary condition to be satisfied at $r = D$. As a result, the solutions to the homogeneous form of equation 5 include incoming and outgoing waves. The complete solution can be written as

$$\bar{p}(\omega, r) = AH_0^1(\zeta r) + BH_0^2(\zeta r) + \frac{\rho_f Z \alpha_{\text{eff}}^2}{L_0}\sigma_0. \quad \text{(A-1)}$$

The coefficients A B are determined from the boundary conditions $\bar{p}(\omega)|_{r=R} = \bar{p}_t(\omega)$ and $\partial\bar{p}/\partial r|_{r=D} = 0$. Applying the boundary conditions, the equation for fluid pressure in the finite fracture can be written as

$$\bar{p}(\omega,r) = \left[\bar{p}_t(\omega) - \frac{\rho_f Z \alpha_{\text{eff}}^2}{L_0}\sigma_0\right] \times \frac{H_0^1(\zeta r)H_1^2(\zeta D) - H_1^1(\zeta D)H_0^2(\zeta r)}{H_0^1(\zeta R)H_1^2(\zeta D) - H_1^1(\zeta D)H_0^2(\zeta R)} + \frac{\rho_f Z \alpha_{\text{eff}}^2}{L_0}\sigma_0. \quad \text{(A-2)}$$

Following similar steps as for an infinite fracture, the expression for the equivalent pressure source for a tube wave, for the finite fracture case, can be obtained as

$$\bar{p}_t(\omega) = \sigma_0 \frac{\omega}{k_r \alpha_f} \frac{c_t}{\alpha_{\text{eff}}} \frac{L_0}{R} \frac{\rho f \alpha_{\text{eff}}^2}{L_0/Z} \times \left[\frac{i\Theta H_1^1(\zeta R)/H_0^1(\zeta R)}{1 + \frac{\omega}{k_r\alpha_f}\frac{c_t}{\alpha_{\text{eff}}}\frac{L_0}{R} i\Theta H_1^1(\zeta R)/H_0^1(\zeta R)}\right], \quad \text{(A-3a)}$$

$$\Theta = \left[1 - \frac{H_1^2(\zeta R)}{H_1^1(\zeta R)}\frac{H_1^1(\zeta D)}{H_1^2(\zeta D)}\right] \Big/ \left[1 - \frac{H_0^2(\zeta R)}{H_0^1(\zeta R)}\frac{H_1^1(\zeta D)}{H_1^2(\zeta D)}\right]. \quad \text{(A-3b)}$$

Using asymptotic expansion of the Hankel functions for large arguments and neglecting higher order terms, Θ can be expanded as

$$\Theta = \frac{1 - e^{i2\zeta(D-R)}}{1 + e^{i2\zeta(D-R)}} = \frac{1 - e^{-2\mathcal{I}_m\{\zeta\}(D-R)}e^{-i2\mathcal{R}_e\{\zeta\}(D-R)}}{1 + e^{-2\mathcal{I}_m\{\zeta\}(D-R)}e^{-i2\mathcal{R}_e\{\zeta\}(D-R)}}. \quad \text{(A-4)}$$

Thus, as $D \to \infty$, Θ goes to unity, and the solution for the finite fracture case approaches the solution for the infinite fracture case as given by equation 8. For the high-frequency approximation, we take the high-frequency solution for the dispersion relation from Tang (1990), and ζ can be written as

$$\zeta = \frac{k_r\alpha_f}{\alpha_{\text{eff}}} = \frac{\omega}{\alpha_{\text{eff}}\left(1 - \sqrt{\frac{i}{2}}\frac{\delta}{L_0}\right)} \approx \frac{\omega}{\alpha_{\text{eff}}}\left[1 + i\frac{\delta}{2L_0}\right]. \quad \text{(A-5)}$$

Using equations A-4 and A-5, $\Theta \approx 1 - 2e^{i2\zeta(D-R)} = 1 - 2e^{-[(\omega\delta/\alpha_{\text{eff}}L_0)(D-R)]}e^{i(2\omega/\alpha_{\text{eff}})(D-R)}$. Thus, the spacing between consecutive peaks/troughs in the high-frequency approximation limit, in Hz, is given by

$$\Delta = \frac{\alpha_{\text{eff}}}{2(D-R)}. \quad \text{(A-6)}$$

The frequency at which the amplitude of the peaks/troughs is 1% of the amplitude ratio from infinite fracture response ω_d is given by

$$2e^{-\left[\frac{\omega_d\delta}{\alpha_{\text{eff}}L_0}(D-R)\right]} = 0.01 \Rightarrow \omega_d = 5.3\frac{\alpha_{\text{eff}}L_0}{\delta(D-R)}. \quad \text{(A-7)}$$

APPENDIX B

TUBE-WAVE ATTENUATION AT A FINITE FRACTURE

As discussed in Appendix A, the solution for a finite fracture involves solving the differential equation for the pressure field in the fracture with a zero flow boundary condition at $r = D$. The solution, including incoming waves and outgoing waves, is given by

$$\bar{p}(r) = \bar{p}_{tt}\frac{H_0^1(\zeta r)H_1^2(\zeta D) - H_1^1(\zeta D)H_0^2(\zeta r)}{H_0^1(\zeta R)H_1^2(\zeta D) - H_1^1(\zeta D)H_0^2(\zeta R)}. \quad \text{(B-1)}$$

From equations B-1 and 3, the flow into the fracture at $r = R$ is given by

$$\bar{q}(R) = \bar{p}_{tt}\zeta\frac{i\omega L_0}{k_r^2\alpha_f^2\rho_f}\frac{H_1^1(\zeta R)}{H_0^1(\zeta R)}\Theta, \quad \text{(B-2)}$$

where Θ is as defined in equation A-3b. Hence, the impedance for a finite fracture can be written as

$$Z_F = \frac{<\bar{p}(R)>}{<\bar{v}_F(R)>} = \frac{\bar{p}_{tt}}{\bar{q}(R)/L_0} = \frac{k_r^2\alpha_f^2\rho_f}{i\omega\zeta}\frac{H_0^1(\zeta R)}{H_1^1(\zeta R)}\frac{1}{\Theta}. \quad \text{(B-3)}$$

Similar to the amplitude ratios in Appendix A, Θ causes peaks/troughs in the transmission coefficient for a finite fracture. At the high-frequency limit, equation A-6 again gives the spacing between consecutive peaks/troughs and equation A-7 gives the frequency at which the amplitude of peaks/troughs in Z_F is reduced to 1%.

REFERENCES

Bandis, S. C., A. C. Lumsden, and N. R. Barton, 1983, Fundamentals of rock joint deformation: International Journal of Rock Mechanics and Mining Sciences and Geomechanics Abstracts, **20**, 249–268, doi: 10.1016/0148-9062(83)90595-8.

Beydoun, W. B., C. H. Cheng, and M. N. Toksöz, 1985, Detection of open fractures with vertical seismic profiling: Journal of Geophysical Research, **90**, 4557–4566, doi: 10.1029/JB090iB06p04557.

Brown, S. R., and X. Fang, 2012, Fluid flow property estimation from seismic scattering data: 82nd Annual International Meeting, SEG, Expanded Abstracts, doi: 10.1190/segam2012-1315.1.

Brown, S. R., and C. H. Scholz, 1985, Broad bandwidth study of the topography of natural rock surfaces: Journal of Geophysical Research, **90**, 12575–12582, doi: 10.1029/JB090iB14p12575.

Burns, D. R., M. E. Willis, M. N. Toksöz, and L. Vetri, 2007, Fracture properties from seismic scattering: The Leading Edge, **26**, 1186–1196, doi: 10.1190/1.2780790.

Cheng, C. H., and M. N. Toksöz, 1982, Generation, propagation and analysis of tube waves in a borehole: Presented at SPWLA 23rd Annual Logging Symposium, 1982-P.

Cicerone, R. D., and M. N. Toksöz, 1995, Fracture characterization from vertical seismic profiling data: Journal of Geophysical Research, **100**, 4131–4148, doi: 10.1029/94JB02982.

Fang, X., M. Fehler, Z. Zhu, Y. Zheng, and D. Burns, 2012, Reservoir fracture characterizations from seismic scattered waves: 82nd Annual International Meeting, SEG, Expanded Abstracts, doi: 10.1190/segam2012-0813.1.

Fehler, M. C., and W. S. Phillips, 1991, Simultaneous inversion for Q and source parameters of microearthquakes accompanying hydraulic fracturing in granitic rock: Bulletin of the Seismological Society of America, **81**, 553–575.
Grandi, S., 2008, Multiscale determination of in situ stress and fracture properties in reservoirs: Ph.D. thesis, Massachusetts Institute of Technology.
Hakami, E., and E. Larsson, 1996, Aperture measurements and flow experiments on a single natural fracture: International Journal of Rock Mechanics and Mining Sciences and Geomechanics Abstracts, **33**, 395–404, doi: 10.1016/0148-9062(95)00070-4.
Hardin, E., 1986, Fracture characterization from attenuation and generation of tube waves: M.S. thesis, Massachusetts Institute of Technology.
Hardin, E. L., C. H. Cheng, F. L. Paillet, and J. D. Mendelson, 1987, Fracture characterization by means of attenuation and generation of tube waves in fractured crystalline rock at Mirror Lake, New Hampshire: Journal of Geophysical Research, **92**, 7989–8006, doi: 10.1029/JB092iB08p07989.
Hornby, B. E., D. L. Johnson, K. W. Winkler, and R. A. Plumb, 1989, Fracture evaluation using reflected Stoneley wave arrivals: Geophysics, **54**, 1274–1288, doi: 10.1190/1.1442587.
Ionov, A. M., 2007, Stoneley wave generation by an incident P-wave propagating in the surrounding formation across a horizontal fluid-filled fracture: Geophysical Prospecting, **55**, 71–82, doi: 10.1111/j.1365-2478.2006.00577.x.
Johnson, D. L., J. Koplik, and R. Dashen, 1987, Theory of dynamic permeability and tortuosity in fluid-saturated porous media: Journal of Fluid Mechanics, **176**, 379–402, doi: 10.1017/S0022112087000727.
Kachanov, M., 1992, Effective elastic properties of cracked solids: Critical review of some basic concepts: Applied Mechanics Reviews, **45**, 304–335, doi: 10.1115/1.3119761.
Kiselevitch, V. L., A. V. Nikolaev, P. A. Troitskiy, and B. M. Shubik, 1991, Emission tomography: Main ideas, results, and prospects: 61st Annual International Meeting, SEG, Expanded Abstracts, 1602.
Kostek, S., D. L. Johnson, and C. J. Randall, 1998a, The interaction of tube waves with borehole fractures, Part I: Numerical models: Geophysics, **63**, 800–808, doi: 10.1190/1.1444391.
Kostek, S., D. L. Johnson, K. W. Winkler, and B. E. Hornby, 1998b, The interaction of tube waves with borehole fractures, Part II: Analytical models: Geophysics, **63**, 809–815, doi: 10.1190/1.1444392.
Lee, M. W., and A. H. Balch, 1982, Theoretical seismic wave radiation from a fluid-filled borehole: Geophysics, **47**, 1308–1314, doi: 10.1190/1.1441391.
Lubbe, R., 2005, A field and laboratory investigation of the fracture compliance of fractured rock: Ph.D. thesis, Oxford University.
Mathieu, F., 1984, Application of full waveform acoustic logging data to the estimation of reservoir permeability: M.S. thesis, Massachusetts Institute of Technology.
Peacock, S., and J. A. Hudson, 1990, Seismic properties of rocks with distributions of small cracks: Geophysical Journal International, **102**, 471–484, doi: 10.1111/j.1365-246X.1990.tb04479.x.
Pyrak-Nolte, L. J., and J. P. Morris, 2000, Single fractures under normal stress: The relation between fracture specific stiffness and fluid flow: International Journal of Rock Mechanics and Mining Sciences & Geomechanics Abstracts, **37**, 245–262, doi: 10.1016/S1365-1609(99)00104-5.
Pyrak-Nolte, L. J., L. R. Myer, and N. G. W. Cook, 1990, Transmission of seismic waves across single natural fractures: Journal of Geophysical Research, **95**, 8617–8638, doi: 10.1029/JB095iB06p08617.
Schoenberg, M., 1980, Elastic wave behavior across linear slip interfaces: Journal of the Acoustical Society of America, **68**, 1516–1521, doi: 10.1121/1.385077.
Tang, X. M., 1990, Acoustic logging in fractured and porous formations: Ph.D. thesis, Massachusetts Institute of Technology.
Tang, X. M., and C. H. Cheng, 1993, Borehole Stoneley wave propagation across permeable structures: Geophysical Prospecting, **41**, 165–187, doi: 10.1111/j.1365-2478.1993.tb00864.x.
Tsang, Y. W., 1984, The effect of tortuosity on fluid flow through a single fracture: Water Resources Research, **20**, 1209–1215, doi: 10.1029/WR020i009p01209.
Tsang, Y. W., and P. A. Witherspoon, 1983, The dependence of fracture mechanical and fluid flow properties on fracture roughness and sample size: Journal of Geophysical Research, **88**, 2359–2366, doi: 10.1029/JB088iB03p02359.
Warpinski, N. R., 2009, Microseismic monitoring: Inside and out: Journal of Petroleum Technology, **61**, 80–85, doi: 10.2118/118537-MS.
White, J., 1983, Underground sound: Application of seismic waves: Elsevier Science.
Willis, M. E., D. R. Burns, R. Rao, B. Minsley, M. N. Toksoz, and L. Vetri, 2006, Spatial orientation and distribution of reservoir fractures from scattered seismic energy: Geophysics, **71**, no. 5, O43–O51, doi: 10.1190/1.2235977.
Witherspoon, P. A., J. S. Y. Wang, K. Iwai, and J. E. Gale, 1980, Validity of cubic law for fluid flow in a deformable rock fracture: Water Resources Research, **16**, 1016–1024, doi: 10.1029/WR016i006p01016.
Worthington, M. H., and R. Lubbe, 2007, The scaling of fracture compliance: : Geological Society, London, Special Publications, **270**, 73–82.
Zimmerman, R., and G. Bodvarsson, 1996, Hydraulic conductivity of rock fractures: Transport in Porous Media, **23**, 1–30, doi: 10.1007/BF00145263.